ELSEVIER

International Journal of Solids and Structures 41 (2004) 4975–4988

INTERNATIONAL JOURNAL OF SOLIDS and STRUCTURES

www.elsevier.com/locate/ijsolstr

Three-dimensional postbuckling and vibration of vertical half-loop under self-weight

R.H. Plaut [a], L.N. Virgin [b,*]

[a] *Department of Civil and Environmental Engineering, Virginia Polytechnic Institute and State University, Blacksburg, VA 24061-0105, USA*

[b] *Department of Mechanical Engineering and Materials Science, Duke University, Durham, NC 27708-0300, USA*

Received 16 March 2004; received in revised form 16 March 2004
Available online 10 May 2004

Abstract

The stability and vibration characteristics of a flexible and inextensible half-loop are investigated. The loop is fixed at two base points, which are separated by a specified distance, and is only subjected to gravity loading. If the length of the loop is sufficiently small, the loop stands upright in a vertical plane. If the length is increased past a critical value, the planar equilibrium shape becomes unstable and the loop droops to one side (i.e., laterally). This out-of-plane displacement may occur smoothly (supercritical bifurcation), or the loop may suddenly jump to a severely-drooped configuration (subcritical bifurcation), depending on the constitutive law. Linearly-elastic and softening materials are considered. Prebuckled and postbuckled equilibrium states are determined numerically with the use of a shooting method. Droop caused by an applied torsional moment is also analyzed. Then small vibrations about the prebuckled (planar) states are studied. Three basic types of vibration modes occur: in-plane, out-of-plane (symmetric), and twist about a vertical axis through the center of the loop. Experiments on a fiber-optic rod and a curtain wire are carried out to qualitatively verify the numerical results for both types of constitutive laws.

Keywords: Buckling; Vibration; Loop; Self-weight; Elastica; Softening

1. Introduction

The three-dimensional deflections of thin elastic rods have been studied in a number of recent papers. Particular attention has been focused on writhing and loop formation when the rods are subjected to tension and torsion (e.g., Goriely and Tabor, 1998; Stump and van der Heijden, 2000; van der Heijden and Thompson, 2000; Stump et al., 2001; Gonzalez et al., 2002; Neukirch et al., 2002), sometimes with application to DNA configurations (e.g., Charitat and Fourcade, 1998; Qian and White, 1998; Stump et al., 1998; Manning and Maddocks, 1999; Furrer et al., 2000; Garrivier and Fourcade, 2000; Panyukov and

* Corresponding author. Tel.: +1-919-660-5342; fax: +1-919-660-8963.
E-mail address: l.virgin@duke.edu (L.N. Virgin).

0020-7683/$ - see front matter © 2004 Elsevier Ltd. All rights reserved.
doi:10.1016/j.ijsolstr.2004.03.014

Rabin, 2000, 2001, 2002; Stump, 2000; Thompson et al., 2002). These rods are often straight in their unstrained state, and also may be circular or helical.

Iooss and Joseph (1990) described a demonstration used by T.B. Benjamin at Oxford University. It involved a curtain wire, which had a tightly-wound steel spring as its core and an outer plastic coating. One end of the wire was pushed upward through a hole in a horizontal board, and then was pushed downward through another hole so the wire formed a half-loop in a vertical plane above the board. More wire was pushed through the first hole, and when the loop attained a critical length, it suddenly drooped to one side. This was cited by Iooss and Joseph (1990) as an example of subcritical bifurcation. Similar behavior of this curtain wire when utilized as a cantilevered column is discussed in Acheson (1997), Fraser and Champneys (2001), Mullin et al. (submitted for publication), and Virgin and Plaut (2004).

This type of half-loop subjected to self-weight is the subject of the present study. It is shown that the bifurcation is supercritical if the loop is linearly-elastic, and subcritical if it has a softening behavior similar to that of the curtain wire. This characteristic also is seen in the column problem (Fraser and Champneys, 2001; Virgin and Plaut, 2004). The analysis of the loop is more complicated due to the large two-dimensional displacements occurring in the prebuckled equilibrium shapes and the large three-dimensional displacements in the postbuckled configurations.

The static problem is formulated in the following section. Then the linearly-elastic case is analyzed in Section 3. In this case the loop is an elastica: inextensible and unshearable, with bending moment proportional to curvature. The dependence of the critical length (and corresponding height) on the weight per unit length is determined. Prebuckled and postbuckled equilibrium shapes are computed using a shooting method. A torsional moment at the supports is considered as an imperfection. In addition, the effect of increasing such an applied moment on the equilibrium shape is examined.

In Section 4, a softening behavior is assumed, and equilibrium paths are obtained again. Vibrations about the stable prebuckled loop are treated in Section 5. Frequencies are plotted as a function of the length of the loop. Experiments are described in Section 6, involving both equilibrium paths and vibrations. A fiber-optic rod and a curtain wire are used to form the loop and to respectively model the linearly-elastic and softening behavior. Concluding remarks are given in Section 7, and an alternative formulation involving Euler angles is presented in Appendix A.

2. Static formulation

The loop is assumed to be elastic and unstrained when straight. Shear deformation, axial deformation, torsional deformation, and rotatory inertia are neglected. A sketch of a planar prebuckled equilibrium shape is shown in Fig. 1a in dimensional terms. The loop is vertical at the supports, which are separated by a distance $2B$. The length of the loop is $2H$ and the constant weight per unit length is W. The cross section is axi-symmetric and the bending stiffness with respect to a diameter of the cross section is EI for the linearly-elastic case.

The arc length is S, the in-plane coordinate X is horizontal, the coordinate Y is vertical, and the coordinate Z points out of the plane. The position vector of a point on the centerline is

$$\mathbf{R}(S) = X(S)\mathbf{i} + Y(S)\mathbf{j} + Z(S)\mathbf{k} \tag{1}$$

and the inextensibility condition is

$$\mathbf{R}' \cdot \mathbf{R}' = 1. \tag{2}$$

The force vector acting on the positive cross section at S is $\mathbf{V}(S)$ and includes the axial force as well as the shear force, unlike the analysis in Stump et al. (2001). Equilibrium of forces provides the vector equation

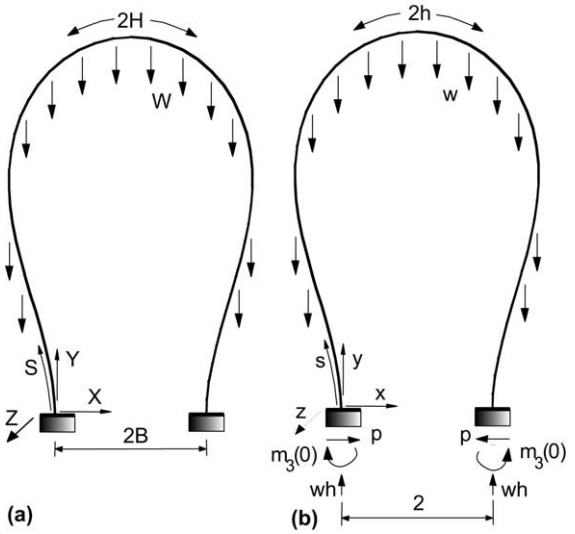

Fig. 1. Geometry of loop subjected to self-weight: (a) dimensional and (b) nondimensional.

$$\mathbf{V}' = W\mathbf{j}. \tag{3}$$

The bending moment vector is $\mathbf{M}(S)$ and acts normal to the cross section at S, and the torsional moment is Q. Equilibrium of moments gives (Stump et al., 2001)

$$(Q\mathbf{R}' + \mathbf{M})' = -\mathbf{R}' \times \mathbf{V}. \tag{4}$$

The moment–curvature relationship is assumed to have the form

$$\left(1 + n\left(\frac{B}{EI}\right)^2 \mathbf{M}\cdot\mathbf{M}\right)\mathbf{M} = EI\mathbf{R}' \times \mathbf{R}'', \tag{5}$$

where $n = 0$ for the linearly-elastic case (i.e., the elastica) as in Stump et al. (2001). For planar deflections of the curtain wire, $n = 4$ provides a good approximation (Virgin and Plaut, 2004).

The analysis is carried out in terms of the following nondimensional quantities:

$$s = \frac{S}{B}, \quad x = \frac{X}{B}, \quad y = \frac{Y}{B}, \quad z = \frac{Z}{B}, \quad h = \frac{H}{B}, \quad \mathbf{r} = \frac{\mathbf{R}}{B}, \quad w = \frac{WB^3}{EI}, \quad \mathbf{v} = \frac{\mathbf{V}B^2}{EI}, \quad q = \frac{QB^2}{EI},$$
$$\mathbf{m} = \frac{\mathbf{M}B}{EI}. \tag{6}$$

Some of these are shown in Fig. 1. Then the governing equations become

$$\begin{aligned} &\mathbf{r}'\cdot\mathbf{r}' = 1,\\ &\mathbf{v}' = w\mathbf{j},\\ &(q\mathbf{r}' + \mathbf{m})' = -\mathbf{r}' \times \mathbf{v},\\ &J\mathbf{m} = \mathbf{r}' \times \mathbf{r}'', \end{aligned} \tag{7}$$

where primes denote differentiation with respect to s, and

$$J = 1 + n(m_1^2 + m_2^2 + m_3^2) \tag{8}$$

in terms of the components of $\mathbf{m}$. Differentiation of the first of Eqs. (7) gives $\mathbf{r}' \cdot \mathbf{r}'' = 0$, and then taking the dot product of the third of Eqs. (7) with $\mathbf{r}'$ and using the derivative of the fourth of Eqs. (7) to get $\mathbf{m}'$ leads to $q' = 0$. Hence the torsional moment q is constant, as previously shown by Stump et al. (2001). Taking the cross product of the fourth of Eqs. (7) with $\mathbf{r}''$ and using the relationship $(\mathbf{a} \times \mathbf{b}) \times \mathbf{c} = (\mathbf{a} \cdot \mathbf{c})\mathbf{b} - (\mathbf{b} \cdot \mathbf{c})\mathbf{a}$, one obtains

$$\mathbf{r}'' = J\mathbf{m} \times \mathbf{r}'. \tag{9}$$

In terms of vector components, Eq. (9) becomes

$$\begin{aligned} x'' &= J(m_2 z' - m_3 y'), \\ y'' &= J(m_3 x' - m_1 z'), \\ z'' &= J(m_1 y' - m_2 x'), \end{aligned} \tag{10}$$

and the third of Eqs. (7) can be written as

$$\begin{aligned} m_1' &= v_2 z' - v_3 y' - q x'', \\ m_2' &= v_3 x' - v_1 z' - q y'', \\ m_3' &= v_1 y' - v_2 x' - q z''. \end{aligned} \tag{11}$$

If p denotes the horizontal reaction shown in Fig. 1b, integration of the second of Eqs. (7) leads to the force components

$$v_1 = -p, \quad v_2 = (s - h)w, \quad v_3 = 0. \tag{12}$$

3. Static analysis of linearly-elastic loop

Equilibrium shapes of the elastica loop are analyzed in this section. Planar, prebuckled equilibrium configurations are considered first. Hence the out-of-plane displacement $z(s)$, the torsional moment q, and the bending moment components $m_1(s)$ and $m_2(s)$ are 0. The governing equations become

$$\begin{aligned} x'' &= -J m_3 y', \\ y'' &= J m_3 x', \\ m_3' &= -p y' - (s - h) w x' \end{aligned} \tag{13}$$

with $J = 1$. The boundary conditions at $s = 0$ are $x = x' = y = 0$ and $y' = 1$, and at the right support where $s = 2h$ they are $x = 2$, $x' = y = 0$, and $y' = -1$.

The computer program Mathematica (Wolfram, 1991) is used to obtain numerical solutions with a shooting method for all problems in this study. Eqs. (13) are written as five first-order equations in x, x', y, y', and m_3. The half-length h and weight w per unit length are specified. The quantities p and $m_3(0)$ are varied until two of the conditions at $s = 2h$ are satisfied with sufficient accuracy; the other two conditions will also be satisfied by the solution.

For $w = 1/32$, the resulting equilibrium shapes are depicted in Fig. 2a–c for $h = 2$, 4, and 6, respectively. The latter two shapes bulge outward near the supports. The central heights for these cases are $y(h) = 1.48$, 3.34, and 5.05, respectively. The critical half-length, h_{cr}, is 6.39.

The solid curves in Fig. 3 demonstrate how the critical half-length h_{cr} and corresponding central height $y(h_{cr})$ decrease as the weight w per unit length is increased. The curves can be approximated by the relationships

$$h_{cr} \approx 2w^{-1/3}, \qquad y(h_{cr}) \approx \tfrac{5}{3} w^{-1/3}. \tag{14}$$

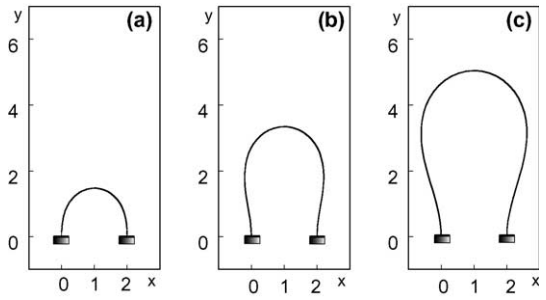

Fig. 2. Prebuckling equilibrium shapes of linearly-elastic loop with $w = 1/32$: (a) $h = 2$, (b) $h = 4$, and (c) $h = 6$.

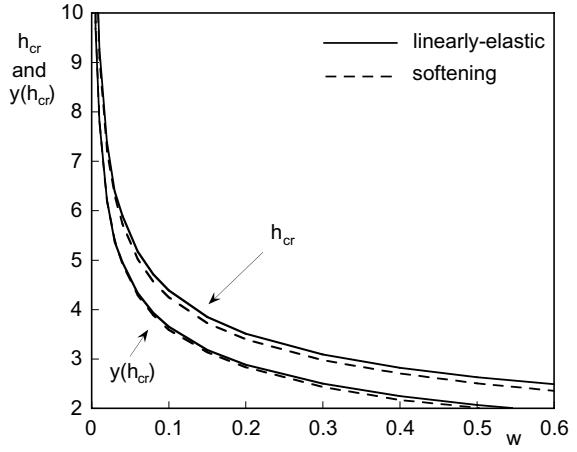

Fig. 3. Critical half-length h_{cr} and corresponding height $y(h_{cr})$ for linearly-elastic loop and softening loop ($n = 4$).

Using (6), one can obtain $H_{cr} \approx 2(EI/W)^{1/3}$ and conclude that for the range shown in Fig. 3, the critical dimensional length $2H_{cr}$ of the loop is essentially independent of the dimensional separation $2B$ of the supports (see Fig. 1). This unexpected result is validated by the experimental results to be described in Section 6.

Nonplanar equilibrium configurations are considered now. Eqs. (10) and (12) are substituted into (11), with $J = 1$. The resulting three equations, along with (10), are written as nine first-order equations. The additional boundary conditions to those for the planar case are $z = z' = m_2 = 0$ at the two supports (at which locations m_2 is not a bending moment component). For fixed values of h, w, and q, the quantities p, $m_1(0)$, and $m_3(0)$ are varied until three of the conditions at $s = 2h$ are satisfied. Alternatively, $m_1(0)$ is fixed and h is varied. This latter approach is applied to compute the critical height when $q = 0$, such as plotted in Fig. 3, with $m_1(0)$ specified as a very small value. It is also useful when the equilibrium paths are almost perpendicular to the h axis.

Equilibrium paths are plotted in Fig. 4 for the case $w = 1/32$ and the range $4 < h < 8$. The abscissa $z(h)$ is the lateral deflection of the center of the loop. For the perfect loop ($q = 0$), which has planar prebuckling shapes, a supercritical bifurcation point occurs at $h_{cr} = 6.39$. (Higher bifurcation points do not appear in the figure.) When the half-length is increased past this point, the planar equilibrium state, with $z(h) = 0$, becomes unstable and the solid nontrivial postbuckling path is followed. The loop droops laterally to one side in a smooth manner.

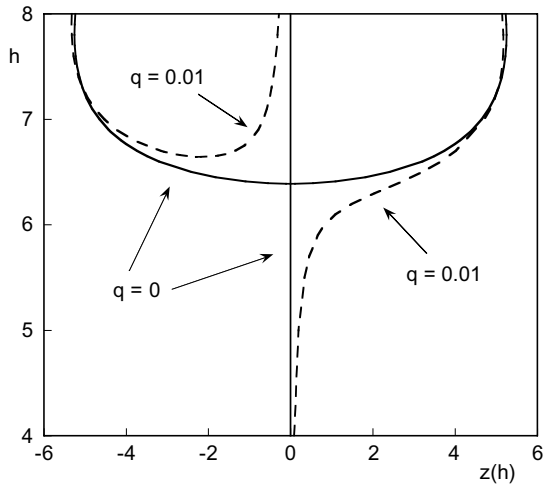

Fig. 4. Equilibrium paths (half-length versus lateral central deflection) for linearly-elastic loop with torsional moment $q = 0$ (perfect case) and $q = 0.01$ (imperfect case).

Perspectives of a planar prebuckled shape and two postbuckled configurations are presented in Fig. 5. Fig. 6 depicts front and side views of three postbuckled shapes. In Fig. 6a and b, $h = 6.6$. The half-length is $h = 7.4$ for Fig. 6c and d, and the front view exhibits two loops. In the formulation used by Stump et al. (2001) and described in Appendix A, one of the Euler angles becomes discontinuous when this occurs, and therefore that formulation was not adopted in the present study. Fig. 6e and f show the postbuckled shape when $h = 9.4$.

Dashed curves in Fig. 4 represent equilibrium paths for the imperfect case having an applied torsional moment $q = 0.01$. Equilibrium states are stable on the primary path on the right side of the figure, and on the left side of the secondary path. The loop does not have a planar equilibrium configuration, and the droop increases smoothly as the length of the loop is increased.

Now consider a given loop (i.e., the length of the loop is fixed), still with $w = 1/32$, and suppose that a torsional moment q is applied at the supports. In Fig. 7, the dependence of the lateral central deflection $z(h)$ on q is plotted for five different half-lengths. If $h = 2$, 3, 4, or 5, $z(h)$ increases as q is increased, within the

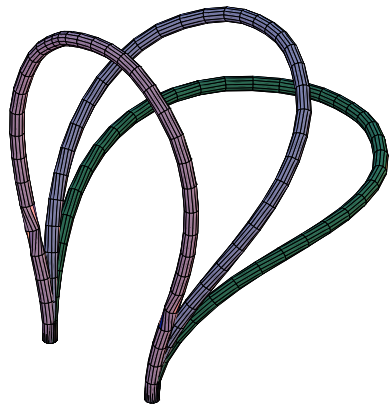

Fig. 5. Equilibrium shapes for prebuckled and postbuckled loop.

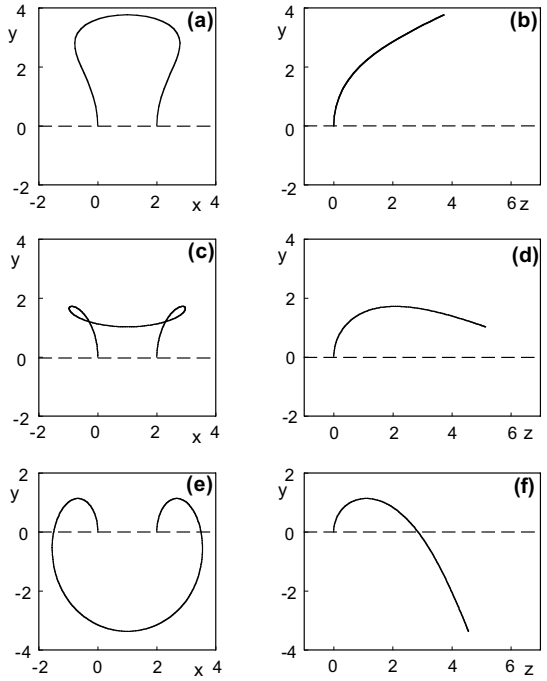

Fig. 6. Postbuckled equilibrium shapes of linearly-elastic loop, front and side views: (a,b) $h = 6.6$; (c,d) $h = 7.4$; (e,f) $h = 9.4$.

range shown. However, if $h = 6$, $z(h)$ reaches a maximum value and then decreases. This latter behavior is similar to that seen in Fig. 6b, d, and f, in which the horizontal deflection of the right end of the curve is greater in Fig. 6d than in Fig. 6b, but smaller in Fig. 6f than in Fig. 6d.

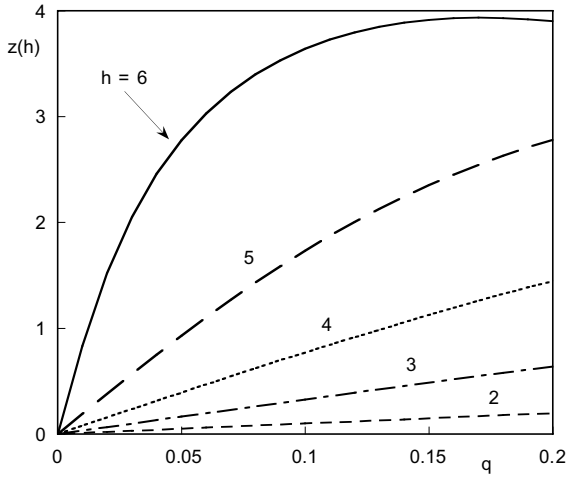

Fig. 7. Lateral central deflection $z(h)$ versus applied torsional moment q.

4. Static analysis of softening loop

In this section, the moment–curvature relationship is given by (5) with $n = 4$. The governing equations for planar and nonplanar equilibrium states are the same as in Section 3 except that J is given by (8) with $n = 4$.

Equilibrium paths are plotted in Fig. 8 for $w = 1/32$ and the range $4 < h < 8$. For the perfect case ($q = 0$), the critical height is $h_{cr} = 6.22$. This is lower than the corresponding value $h_{cr} = 6.39$ for the linearly-elastic loop (i.e., when $n = 0$). For the cantilevered column treated in Virgin and Plaut (2004), the critical height was the same for linearly-elastic and softening cases, because the prebuckled (straight) configuration was not affected by the constitutive law. For the loop, the prebuckled shapes are not the same for the two cases, and hence the critical heights are not the same.

When $n = 4$, as seen in Fig. 8, the bifurcation is subcritical, with the initial postbuckling path falling. The nontrivial equilibrium states are unstable on this falling portion, i.e., until the minimum point is reached, and then become stable as the path rises. If the half-length h of the prebuckled loop with $w = 1/32$ is increased and reaches h_{cr}, the loop jumps suddenly from the planar configuration to the severely-drooped shape depicted in Fig. 9. This is the behavior observed in Benjamin's demonstration (Iooss and Joseph, 1990), and is quite different from that of the linearly-elastic loop analyzed in the previous section.

On the primary imperfect path on the right side of Fig. 8 with $q = 0.01$, a jump in the shape occurs when the maximum (limit) point is reached. The sudden change in the amount of droop is smaller than for the perfect loop. For this case, in which the postbuckling path falls initially but then rises, if the imperfection were sufficiently large, the primary equilibrium path would not have any turning points and the equilibrium shapes would change smoothly as the loading parameter is increased.

For the softening loop, the dashed curves in Fig. 3 show the effect of the weight w per unit length on the critical half-length and corresponding central height. The values are slightly lower than those for the linearly-elastic loop. Again, the ordinates are approximately proportional to $w^{-1/3}$, and (for given bending stiffness EI and dimensional weight W per unit length) the dimensional critical length $2H_{cr}$ is almost independent of the support separation $2B$ over the range shown in the figure.

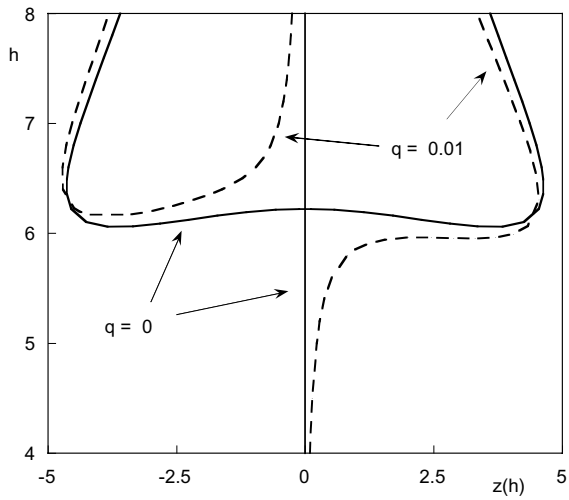

Fig. 8. Equilibrium paths for softening loop with torsional moment $q = 0$ and $q = 0.01$.

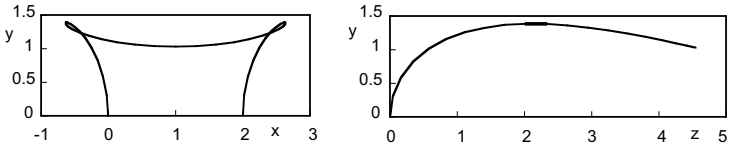

Fig. 9. Postbuckled equilibrium shape of softening loop at h_{cr}, front and side views.

5. Vibrations of linearly-elastic loop

Small vibrations about the planar prebuckled configurations of the linearly-elastic loop are investigated in this section. The analysis is carried out in nondimensional terms. If ω denotes the dimensional frequency and T is dimensional time, then the corresponding nondimensional quantities are

$$\Omega = \omega B^2 \sqrt{\frac{W}{EIg}}, \qquad t = \frac{T}{B^2}\sqrt{\frac{EIg}{W}}. \tag{15}$$

Eqs. (10) and (11) are valid, where primes now denote partial differentiation with respect to s, and the second of Eqs. (7) is replaced by the component equations

$$v_1' = \frac{\partial^2 x}{\partial t^2}, \quad v_2' = w + \frac{\partial^2 y}{\partial t^2}, \quad v_3' = \frac{\partial^2 z}{\partial t^2}. \tag{16}$$

The variables $x(s,t)$, $y(s,t)$, $z(s,t)$, $m_1(s,t)$, $m_2(s,t)$, $m_3(s,t)$, $v_1(s,t)$, $v_2(s,t)$, $v_3(s,t)$, and $q(t)$ are written in terms of an equilibrium component and a dynamic component (vibration mode) having frequency Ω:

$$\begin{aligned}
&x(s,t) = x_e(s) + x_d(s)\sin\Omega t,\\
&y(s,t) = y_e(s) + y_d(s)\sin\Omega t,\\
&z(s,t) = z_e(s) + z_d(s)\sin\Omega t,\\
&m_j(s,t) = m_{je}(s) + m_{jd}(s)\sin\Omega t \quad (j = 1,2,3),\\
&v_j(s,t) = v_{je}(s) + v_{jd}(s)\sin\Omega t \quad (j = 1,2,3),\\
&q(t) = q_d \sin\Omega t.
\end{aligned} \tag{17}$$

The static torsional moment is 0 for the equilibrium states under consideration, as are z_e, m_{1e}, m_{2e}, and v_{3e}. Eqs. (17) are substituted into (10), (11), and (16). The equilibrium components satisfy (12) and (13) with $J = 1$. The nonlinear terms in the dynamic components are neglected, and the coefficients of $\sin\Omega t$ provide the remaining governing equations. The boundary conditions on the modal quantities at $s = 0$ and $s = 2h$ are $x_d = x_d' = y_d = y_d' = z_d = z_d' = m_{2d} = 0$.

Three basic types of vibration occur. The equations involving the modal variables separate into two sets. One set is associated with in-plane vibrations. The other set leads to the remaining two types of vibration. One involves out-of-plane symmetric lateral vibrations, and the other involves twisting vibrations about a vertical line through the apex of the loop. Perspectives of these forms are presented in Fig. 9, where the light shape is the planar equilibrium configuration and the dark shape is the first mode for each of the three types. Similar vibration behavior was described in Molloy et al. (1999) for two arch-shells that lean against each other.

For in-plane vibration modes, $z_d = m_{1d} = m_{2d} = v_{3d} = 0$ and the equations are

$$\begin{aligned} x_d'' &= -m_{3e}y_d' - m_{3d}y_e', \\ y_d'' &= m_{3e}x_d' + m_{3d}x_e', \\ m_{3d}' &= -py_d' + v_{1d}y_e' - (s-h)wx_d' - v_{2d}x_e', \\ v_{1d}' &= -\Omega^2 x_d, \\ v_2' &= -\Omega^2 y_d. \end{aligned} \tag{18}$$

The dynamic torsional moment amplitude q_d does not appear, since $z_e'' = 0$. Eqs. (13), with subscripts e added to the variables, and Eqs. (18) are written as a set of 12 first-order equations. Values of p and $m_3(0)$ are found from the previous equilibrium solution (Section 3). One of the three unknown conditions $m_{3d}(0)$, $v_{1d}(0)$, and $v_{2d}(0)$ is given a certain (arbitrary) magnitude, and the other two are varied, along with the frequency Ω, until three of the conditions at $s = 2h$ are satisfied.

Numerical results are obtained for $w = 1/32$. The variations of the lowest two in-plane frequencies with the half-length are shown by the dashed curves in Fig. 11. All the frequencies decrease as h increases in the range shown ($2 < h < h_{cr} = 6.39$). The lowest in-plane frequency is asymmetric and has a node near the center of the loop, as sketched in Fig. 10b. The second in-plane mode is symmetric and has two nodes.

For the other two types of vibration, the modal quantities x_d, y_d, m_{3d}, v_{1d}, and v_{2d} are 0. The equations involving the modal variables are

$$\begin{aligned} z_d'' &= m_{1d}y_e' - m_{2d}x_e', \\ m_{1d}' &= (s-h)wz_d - v_{3d}y_e' + q_d m_{3e}y_e', \\ m_{2d}' &= v_{3d}x_e' + pz_d' - q_d m_{3e}x_e', \\ v_{3d}' &= -\Omega^2 z_d, \end{aligned} \tag{19}$$

where (13) with $J = 1$ has been used to replace x_e'' and y_e'' in the last terms of the middle two equations of (19). Eqs. (13) and (19) lead to 10 first-order equations.

One type of vibration will be called "out-of-plane". These mode shapes are symmetric in the front view. One of the four shooting conditions is chosen as $m_{1d}(2h) = -m_{1d}(0)$ to obtain these symmetric modes. The fundamental mode of this type is sketched in Fig. 10a and has no node (i.e., it droops to one side and then the other as it vibrates). The lateral deflection functions $z_d(s)$ are similar in form to the symmetric vibration modes of a fixed–fixed beam. The second out-of-plane mode $z_d(s)$ has two nodes. The solid curves in Fig. 11

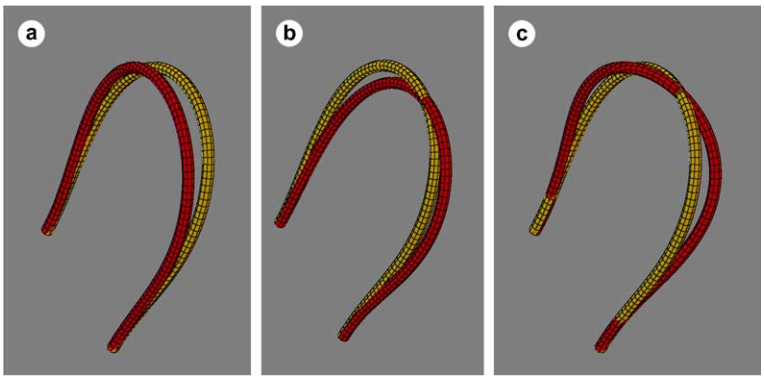

Fig. 10. Fundamental modes for (a) out-of-plane, (b) in-plane, and (c) twisting vibrations.

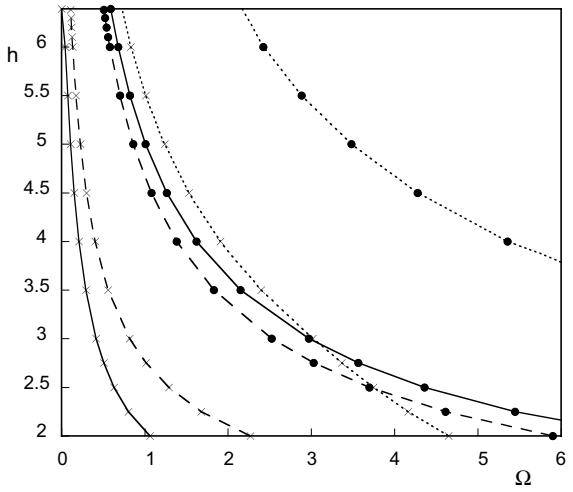

Fig. 11. Half-length versus lowest two frequencies of each type. (—) out-of-plane; (- - - -) in-plane; (···) twist.

show how the first two out-of-plane frequencies vary with h when $w = 1/32$. The fundamental one is the lowest of all the frequencies and decreases to 0 at the critical height (where the corresponding vibration mode becomes the buckling mode).

The last type of vibration will be called "twist". Fig. 10c depicts the fundamental mode of this type. Here the shooting condition $m_{1d}(2h) = m_{1d}(0)$ is included. For small half-lengths h, the twist mode shapes $z_d(s)$ are similar to the anti-symmetric modes of a fixed–fixed beam. However, as h increases, an additional node appears near $s = 0$ and near $s = 2h$, so that the fundamental twist mode has three nodes and the second twist mode has five nodes. For the case $w = 1/32$, the dotted curves in Fig. 11 demonstrate that the fundamental twist frequency is higher than the fundamental out-of-plane and in-plane frequencies, and is also higher than the second frequencies of those other types if h is sufficiently large.

6. Experiments

A brief study was conducted of a loop made of a linearly-elastic material. A single fiber-optic rod was chosen due its flexibility and dimensions. Fig. 12 shows some typical results. In part (a) is shown the

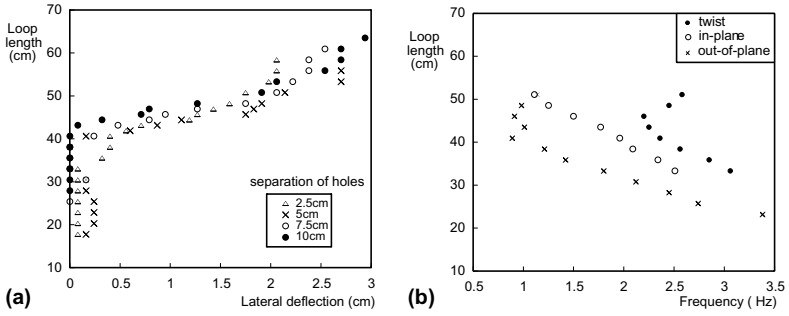

Fig. 12. Behavior of loop made of fiber-optic rod: (a) equilibrium paths (length versus lateral central deflection); (b) lowest frequencies for the three types of vibration.

horizontal (lateral) deflection of the centerpoint of the loop as the length is increased. The data points correspond to a loop in which the separation of the base holes varies from 2.5 to 10 cm. In all these cases the loop retains its upright (trivial) equilibrium until the length has been extended to about 40 cm. At this point the loop begins to gradually droop to one side. This is a supercritical pitchfork bifurcation. In part (b) the averaged results of three vibration tests (for the 5 cm hole separation) show how the lowest frequency in each mode varied as the length of the cable was changed. The ordering of the frequencies is the same as in the theoretical results, and an increase in frequency can also be observed as the rod enters the postbuckled regime. However, the frequency data were not acquired to a high degree of accuracy and hence a quantitative comparison with theory is not appropriate.

A series of tests were conducted with the softening curtain wire. Four sets of hole separation were used: 10, 15, 20, and 25 cm. For each case the length of the cable was increased and the lateral deflection was measured a short distance up from the base. The experimental system is shown in three stages of deformation in Fig. 13. In a uniform gravitational field the loop will reach a critical value, at which it flops suddenly to one side (unlike the linearly-elastic loop which exhibits a continuous change of out-of-plane deformation). Fig. 14a shows the measured (equilibrium) results. In each case a sudden jump to a severely-drooped configuration is apparent. In this case the cable length is scaled by the hole separation. Frequencies were also measured (using a laser velocity vibrometer) and these are shown for a hole separation of 20 cm in Fig. 14b. Frequencies became increasingly difficult to measure very close to the critical length due to the shrinking nature of the attractive domain of initial conditions surrounding the equilibrium state. Also, since the stiffness is decreasing, so too is the damping *ratio* and motion becomes increasingly sluggish (especially for the twisting motion).

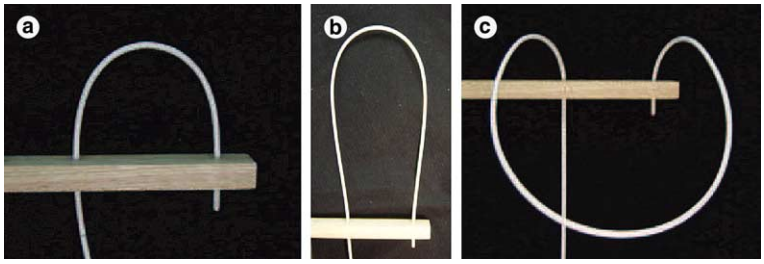

Fig. 13. Front view of loop: (a) small h, prebuckled; (b) large h, prebuckled; (c) postbuckled.

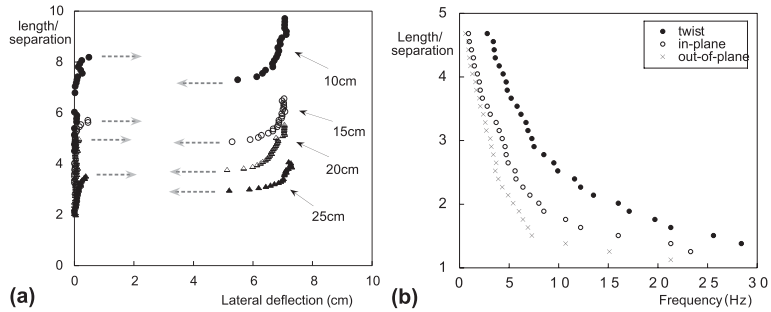

Fig. 14. Behavior of loop made of curtain wire: (a) equilibrium paths (h versus lateral deflection 5 cm above supports); (b) lowest frequencies for the three types of vibration.

7. Concluding remarks

This is a companion paper to Virgin and Plaut (2004), which studied the classical problem of a cantilevered column under self-weight but included a softening material as well as a linearly-elastic material. The bifurcation behavior at the critical height may be subcritical for a softening moment–curvature relationship, leading to a sudden jump from the prebuckled state to a postbuckled configuration. This is different from the usual postbuckling behavior of linearly-elastic columns, and was previously discussed by Fraser and Champneys (2001).

A similar phenomenon was investigated here for a flexible loop standing upright (when sufficiently short) above two fixed supports. The demonstration described in Iooss and Joseph (1990) exhibited a sudden jump to a severely-drooped configuration when the length of the loop reached its critical value. The loop they described had a softening behavior, and it was shown here that a linearly-elastic loop would have a smooth transition from the planar shape to drooped (nonplanar) shapes.

Linearly-elastic loops and softening loops with a behavior similar to that of the curtain wire used in the experiments were analyzed. The governing equations were formulated, critical loads were determined, prebuckled and postbuckled equilibrium configurations were obtained, an applied torsional moment was considered, and small vibrations about prebuckled states of the linearly-elastic loop were computed.

For the parameters considered, it was found that the critical length of the loop is almost independent of the separation between the supports (within a large range of separations). This was a surprising result. The critical lengths and corresponding heights of the softening loop were found to be slightly smaller than those for the linearly-elastic loop. Three types of vibration modes were found, with a symmetric droop mode yielding the lowest fundamental frequency.

The experiments involved loops made of a linearly-elastic fiber-optic rod and a softening curtain wire. Four different support separations were used for each material. The prebuckling, postbuckling, and vibration characteristics exhibited in the tests were qualitatively similar to those obtained in the analytical and numerical work.

Acknowledgements

The authors are grateful to Stacia S. Keller at Virginia Tech for carrying out some of the computations, and to R. Ben Davis at Duke University for assisting with the experiments. They also acknowledge helpful comments from the reviewers.

Appendix A. Alternative form using Euler angles

For the linearly-elastic loop, equilibrium shapes can be obtained using the formulation in Stump et al. (2001). It involves Euler angles ϕ and θ, and will be presented in nondimensional terms.

For planar configurations, $\phi(s)$ is the angle from the x axis to the loop tangent. For example, $\phi(0) = \pi/2$, $\phi(h) = 0$, and $\phi(2h) = -\pi/2$ in Fig. 1b. For three-dimensional shapes, ϕ again is measured in the xy plane and has the same interpretation relative to the projection of the loop. The angle $\theta(s)$ is measured from the xy plane to the loop tangent at s. Therefore $\theta(s)$ is identically 0 for planar shapes, and $\theta(0) = \theta(2h) = 0$ for nonplanar shapes.

From geometrical considerations,

$$x' = \cos\theta\cos\phi, \quad y' = \cos\theta\sin\phi, \quad z' = \sin\theta. \tag{A.1}$$

The equilibrium equations in terms of ϕ and θ are

$$\begin{aligned}\phi''\cos\theta &= 2\phi'\theta'\sin\theta-(s-h)w\cos\phi-p\sin\phi-q\theta',\\ \theta'' &= -\left[(\phi')^2\cos\theta-(s-h)w\sin\phi+p\cos\phi\right]\sin\theta+q\phi'\cos\theta.\end{aligned} \tag{A.2}$$

For planar configurations, $z(s)=\theta(s)=q=0$ and the governing equations reduce to

$$\begin{aligned}x' &= \cos\phi,\quad y'=\sin\phi,\\ \phi'' &= -(s-h)w\cos\phi-p\sin\phi.\end{aligned} \tag{A.3}$$

For nonplanar shapes, application of the shooting method becomes difficult when loops form in the front view (see Figs. 6c and 9a). If $w=1/32$, this occurs when h reaches 7.12. The angle θ passes through the value $\pi/2$, which causes the first of Eqs. (A.2) to be singular.

References

Acheson, D., 1997. From Calculus to Chaos: An Introduction to Dynamics. Oxford University Press, Oxford, UK.

Charitat, T., Fourcade, B., 1998. Metastability of a circular o-ring due to intrinsic curvature. Eur. Phys. J B1, 333–336.

Fraser, W.B., Champneys, A.R., 2001. The 'Indian rope trick' for a parametrically excited flexible rod: nonlinear and subharmonic analysis. Proc. R. Soc. Lond. A 458, 1353–1373.

Furrer, P.B., Manning, R.S., Maddocks, J.H., 2000. DNA rings with multiple energy minima. Biophys. J. 79, 116–136.

Garrivier, D., Fourcade, B., 2000. Twisting DNA with variable intrinsic curvature. Europhys. Lett. 49, 390–395.

Gonzalez, O., Maddocks, J.H., Schuricht, F., von der Mosel, H., 2002. Global curvature and self-contact of nonlinearly elastic curves and rods. Calc. Var. Partial Diff. Eqs. 14, 29–68.

Goriely, A., Tabor, M., 1998. Nonlinear dynamics of filaments; IV: spontaneous looping of twisted elastic rods. Proc. R. Soc. Lond. A 454, 3183–3202.

Iooss, G., Joseph, D.D., 1990. In: Elementary Stability and Bifurcation Theory, 2nd ed. Springer-Verlag, New York, pp. 22–24.

Manning, R.S., Maddocks, J.H., 1999. Symmetry breaking and the twisted elastic ring. Comp. Meth. Appl. Mech. Engng. 170, 313–330.

Molloy, S.J., Plaut, R.H., Kim, J.-Y., 1999. Behavior of pair of leaning arch-shells under snow and wind loads. J. Engng. Mech. 125, 663–667.

Mullin, T., Champneys, A., Fraser, W.G., Galan, J., Acheson, D., submitted for publication. The 'Indian rod trick' via parametric excitation.

Neukirch, S., van der Heijden, G.H.M., Thompson, J.M.T., 2002. Writhing instabilities of twisted rods: from infinite to finite length. J. Mech. Phys. Solids 50, 1175–1191.

Panyukov, S., Rabin, Y., 2000. Fluctuating filaments: statistical mechanics of helices. Phys. Rev. E (Pt. B) 62, 7135–7146.

Panyukov, S., Rabin, Y., 2001. Fluctuating elastic rings: statics and dynamics. Phys. Rev. E (Pt. 1) 64, 011909/1–011909/19.

Panyukov, S., Rabin, Y., 2002. On the deformation of fluctuating chiral ribbons. Europhys. Lett. 57, 512–518.

Qian, H., White, J.H., 1998. Terminal twist induced continuous writhe of a circular rod with intrinsic curvature. J. Biomolec. Struc. Dyn. 16, 663–669.

Stump, D.M., 2000. Toroidal supercoiling of writhed rods. Proc. R. Soc. Lond. A 456, 1979–1995.

Stump, D.M., van der Heijden, G.H.M., 2000. Matched asymptotic expansions for bent and twisted rods: applications for cable and pipeline laying. J. Engng. Math. 38, 13–31.

Stump, D.M., Fraser, W.B., Gates, K.E., 1998. The writhing of circular cross-section rods: undersea cables to DNA supercoils. Proc. R. Soc. Lond. A 454, 2123–2156.

Stump, D.M., Champneys, A.R., van der Heijden, G.H.M., 2001. The torsional buckling and writhing of a simply supported rod hanging under gravity. Int. J. Solids Struct. 38, 795–813.

Thompson, J.M.T., van der Heijden, G.H.M., Neukirch, S., 2002. Supercoiling of DNA plasmids: mechanics of the generalized ply. Proc. R. Soc. Lond. A 458, 959–985.

van der Heijden, G.H.M., Thompson, J.M.T., 2000. Helical and localised buckling in twisted rods: a unified analysis of the symmetric case. Non. Dyn. 21, 71–99.

Virgin, L.N., Plaut, R.H., 2004. Postbuckling and vibration of linearly-elastic and softening columns under self-weight. Int. J. Solids Struct.

Wolfram, S., 1991. Mathematica: A System for Doing Mathematics by Computer. Addison-Wesley, Reading, MA.